Challenges and benefits of using NO_x as a quantitative proxy for fossil fuel CO_2 in an urban area based on radiocarbon measurements

Hannes Juchem[1,2], Fabian Maier[3], Ingeborg Levin[1,†], Armin Jordan[4], Denis Pöhler[1,5], Claudius Rosendahl[1], Julian Della Coletta[1,2], Susanne Preunkert[1,2], and Samuel Hammer[1,2]

[1]Institute of Environmental Physics, Heidelberg University, INF 229, 69120 Heidelberg, Germany
[2]ICOS Central Radiocarbon Laboratory, Heidelberg University, Berliner Straße 53, 69120 Heidelberg, Germany
[3]Max Planck Institute for Biogeochemistry, 07745 Jena, Germany
[4]ICOS Flask and Calibration Laboratory, Max Planck Institute for Biogeochemistry, 07745 Jena, Germany
[5]Airyx GmbH, Hans-Bunte-Str. 4, 69123 Heidelberg, Germany
[†]deceased, 10 February 2024

Correspondence: Hannes Juchem (hjuchem@iup.uni-heidelberg.de)

Abstract. Radiocarbon ($^{14}CO_2$) observations are the benchmark for quantifying fossil fuel CO_2 ($ffCO_2$) in the atmosphere, but continuous $^{14}CO_2$ measurements are not yet available. Continuous estimates of $ffCO_2$ can be made by observing continuously measurable proxies that are co-emitted during fossil fuel combustion. This paper investigates the potential and challenges of using in situ NO_x observations in urban areas to quantitatively estimate hourly $ffCO_2$ enhancements, in the example of the ICOS pilot station in Heidelberg, Germany. The short atmospheric lifetime of NO_x limits the use of the observed signal to a local area. Thus, a local NO_x and $ffCO_2$ background was approximated using the Stochastic Time-Inverted Lagrangian Transport (STILT) model and bottom-up emission estimates from the Netherlands Organisation for Applied Scientific Research (TNO). Using $^{14}CO_2$ data from 185 hourly integrated flask samples between 2020 and 2021, mean ratios of local excess NO_x (ΔNO_x) to local excess $ffCO_2$ ($\Delta ffCO_2$) of $1.40\,\mathrm{ppb\,ppm^{-1}}$ for winter and $2.12\,\mathrm{ppb\,ppm^{-1}}$ for summer were calculated. These ratios were applied to the ΔNO_x time series to construct continuous $\Delta ffCO_2$ estimates. The uncertainty of the ΔNO_x-based $\Delta ffCO_2$ record was estimated at $3.94\,\mathrm{ppm}$. Comparisons with $^{14}CO_2$-based and ΔCO-based $\Delta ffCO_2$ estimates showed good agreement, while still demonstrating distinct behaviour for individual events. ΔNO_x shows considerable potential as $\Delta ffCO_2$ proxy and as useful addition to ΔCO-based estimates, as both proxies have different footprints due to their lifetimes. A key challenge remains in reliably determining the seasonal and diurnal cycle of average ΔNO_x to $\Delta ffCO_2$ ratios.

1 Introduction

To derive top-down estimates of anthropogenic CO_2 emissions due to fossil fuel combustion from atmospheric measurements, it is necessary to separate the recently added biospheric and fossil fuel CO_2 ($ffCO_2$) signal (Ciais et al., 2015). The most direct method to derive these excess fossil fuel CO_2 contributions ($\Delta ffCO_2$, the term "excess" is used to describe an enhancement of the measured signal above a given background level) is by utilising $^{14}CO_2$ measurements compared to a background site

(Levin et al., 2003; Turnbull et al., 2006). However, at present, optical methods for continuous ^{14}C measurements are just developing (Ling et al., 2025), and existing methods like accelerator mass spectrometry (AMS) and low level counting (LLC) work only on discrete samples and are labour intensive. Continuously measured species that are co-emitted in combustion processes, such as CO or NO_x, are a possible alternative for deriving high temporal resolution $ffCO_2$ estimates (Turnbull et al., 2006; Levin and Karstens, 2007; Van Der Laan et al., 2010; Maier et al., 2024a). These have the advantage of lower-cost continuous measurements, are in part (CO and NO_2) observable by satellite (Konovalov et al., 2016), and in urban areas can even outperform sparsely collected ^{14}C-based estimates in inversion modelling (Maier et al., 2024b). However, they require adequate knowledge about the ratio of excess proxy concentrations to $\Delta ffCO_2$. For readability purposes, the manuscript used the simplification 'concentration' for the mole fraction of the respective molecule, even though, strictly speaking, this is incorrect when using ppm units.

CO has already been widely studied as a proxy for $\Delta ffCO_2$ (Gamnitzer et al., 2006; Levin and Karstens, 2007; Turnbull et al., 2015; Maier et al., 2024a). Using NO_x as a proxy has been the subject of considerably less study, with the majority of research conducted using satellite data and ratios derived from inventories (Lopez et al., 2013; Goldberg et al., 2019; Liu et al., 2020; Feng et al., 2024). A fundamental challenge of both proxies is that CO and NO_x emissions depend on fuel type and combustion parameters like e.g. combustion temperature, oxygen supply, and applied emission reduction systems. Accordingly, different emission sectors, like traffic, industry, and residential heating, have different average proxy to $ffCO_2$ emission ratios, which also vary within the emission sectors. The use of NO_x is accompanied by additional challenges due to its atmospheric chemistry and its relatively short atmospheric lifetime, which is on the order of hours (Beirle, 2004).This implies that atmospheric $\frac{\Delta NO_x}{\Delta ffCO_2}$ ratios vary by station and reflect the composition of fossil fuel sources present in each station's footprint. These features can also be an advantage, as it gives the NO_x signal a more localised nature and generally a low background (Goldberg et al., 2019), which also means that it quickly adapts to changes in emissions. Therefore, NO_x is a promising proxy for urban applications and constraining city-wide emissions. Furthermore, the combination of multiple proxies can provide better constraints on fossil fuel emissions and enable attribution of emissions to source sectors (Super et al., 2020; Jaschke, 2021).

This study characterises the potential and challenges of using NO_x concentration excesses (ΔNO_x) from in situ observations as a proxy for $\Delta ffCO_2$ in an urban setting by deriving $\frac{\Delta NO_x}{\Delta ffCO_2}$ ratios from radiocarbon measurements, using Heidelberg as an example. While the absolute $\frac{\Delta NO_x}{\Delta ffCO_2}$ ratios are likely to differ for other urban areas and need to be determined on a per-site basis, the general approach for considering the local nature of the measured NO_x signal is applicable to other cities and the associated uncertainties serve as an indicator of the uncertainties likely to be encountered in other urban environments. As NO_x shows a much more localised signal than CO and ^{14}C, the choice of a suitable and common background for both species is highly important. In the absence of a suitable NO_x and $^{14}CO_2$ measurement station to define a local background, we describe its construction based on forward simulations of European NO_x and $ffCO_2$ emissions in the Stochastic Time-Inverted Lagrangian Transport model (STILT, Lin et al. (2003)) and discuss the associated additional uncertainties. Following the methodology of Maier et al. (2024a), the ratios of ΔNO_x to $\Delta ffCO_2$ concentrations obtained from in situ NO_x and flask-based ^{14}C measurements are then analysed for diurnal and seasonal variation, to determine average atmospheric $\frac{\Delta NO_x}{\Delta ffCO_2}$ ratios. With these, ΔNO_x-based $\Delta ffCO_2$ estimates are calculated and benchmarked against ^{14}C-based $\Delta ffCO_2$ estimates to assess

the accuracy of the proxy. We investigate what share of the ΔNO_x-based $\Delta ffCO_2$ uncertainty is due to the observation and background uncertainty and what is due to the inherent oversimplification of applying observation-based seasonally averaged $\frac{\Delta NO_x}{\Delta ffCO_2}$ ratios. The ΔNO_x-based continuous $\Delta ffCO_2$ record is compared to a ΔCO-based record in order to analyse if and how the two proxies differ. Finally, both proxy-based $\Delta ffCO_2$ records are compared to an independent $^{14}CO_2$-based $\Delta ffCO_2$ record with fortnightly resolution for Heidelberg.

2 Methods

2.1 Site and data description

Heidelberg is a city with a population of approximately 160,000, situated in the densely populated Upper Rhine Valley in south-western Germany. The measurement site is located in the northern part of the city, within the university campus. The sampling intake for the measurements is located $30\ \mathrm{m}$ above ground on the roof of the Institute for Environmental Physics, approximately $100\ \mathrm{m}$ from a residential area and a high traffic road, with little traffic directly around the building. Thus, local emissions of CO_2 and NO_x are predominantly attributable to traffic and residential heating. A combined heat and power station, with a chimney height of $120\ \mathrm{m}$, is situated $500\ \mathrm{m}$ to the north of the site, while a cement plant is located approximately $7\ \mathrm{km}$ to the south. Moreover, the cities of Mannheim and Ludwigshafen, which are characterised by a high degree of industrialisation, are situated approximately $15 - 20\ \mathrm{km}$ to the north-west. These include a large coal-fired power plant and the BASF industrial complex. Furthermore, air masses originating from the southern part of the Rhine Valley frequently affect the station due to the predominant south-westerly winds in Western Europe, which are further pronounced by the channelling effect of the Rhine Valley.

Continuous measurements of atmospheric CO_2 concentrations are performed with a Cavity Ring-Down Spectroscopy (CRDS) gas analyser (Picarro G2401). The measurement protocol as well as the calibration are in accordance with the ICOS Atmosphere Station specifications Version 2.0 (ICOS RI, 2020). The data processing is performed via the ICOS Atmosphere Thematic Center (ATC) following Hazan et al. (2016). NO_x concentrations are measured with an iterative cavity-enhanced DOAS (ICAD) instrument. The ICAD measures absorption spectra and determines the in situ NO_2 concentration by fitting its characteristic absorption structures. NO_x is measured by converting NO to NO_2 through the addition of ozone (Horbanski et al., 2019). An ICOS flask sampler is used to collect flask samples integrated over one hour (see Levin et al. (2020) for a description of the sampler). The flow of air into the flasks is controlled by mass flow controllers so that the final sample in the flask approximates a one hour average of the concentrations in the ambient air. The flask samples are measured for CO_2 concentrations at the ICOS Flask and Calibration Laboratory (FCL, https://www.icos-cal.eu/fcl) with a gas chromatographic analysis system (GC) (Jordan and Damak, 2025). Subsequently, the CO_2 in the flasks is extracted and graphitized at the Central Radiocarbon Laboratory (CRL, https://www.icos-cal.eu/crl; Lux (2018)) for subsequent ^{14}C analysis with an accelerator mass spectrometer (AMS, Kromer et al. (2013)). Additionally, integrated CO_2 sampling using NaOH solution has been implemented at HEI station since the late 1970s. Fortnightly samples are collected between 19:00 and 7:00 local time and analysed for ^{14}C at the CRL

(Levin et al., 1980; Kromer and Münnich, 1992). In 2013 a second integrated sampling device for afternoon hours between 11:00 and 16:00 was added.

More than 600 flask samples were collected and analysed for ^{14}C in the years 2019 to 2021, covering a variety of atmospheric situations (Maier, 2023). The samples cover most of the day, especially the morning and evening rush hours, as well as the afternoon and night. The flasks were analysed following the same procedure as in Maier et al. (2024a). Accordingly, flasks with a modelled nuclear contamination from $^{14}CO_2$ emissions of nuclear facilities above $2‰$ were excluded to avoid high nuclear corrections with uncertainties exceeding typical ^{14}C uncertainties. NO_x measurements are available from 18.12.2019 on. Multiple periods of one to four weeks in March, June, July, and October 2020, as well as March and July in 2021, were excluded due to instrument outages or maintenance. NO_x data is available for 246 of the flask sampling periods. In the following, all times are given in local time, as we expect this to be better suited than UTC to capture and explain the patterns of human behaviour and diurnal cycles, that affect the emission ratios.

2.2 Construction of a suitable background

To calculate the excess concentration of a species, the background concentration must be subtracted from the measured concentration. For estimating ^{14}C- or CO-based $ffCO_2$ excess concentrations, the marine sector of the ICOS station at Mace Head (MHD), located on the west coast of Ireland, is a suitable choice for assessing European background conditions, due to the prevailing westerlies (Maier et al., 2023, 2024a). Maier et al. (2023) investigated the additional $ffCO_2$ uncertainties that arise from the approximation of the European background concentrations based on the clean air sector in MHD and quantified these at $0.28\ \mathrm{ppm}$. However, due to atmospheric chemistry, the lifetime of NO_x is on the order of hours (Beirle, 2004), and thus removal of NO_x from the atmosphere becomes important on scales larger than the immediate vicinity of the measurement site. This prevents the use of MHD as a NO_x background station. Exploiting the co-emission link between $ffCO_2$ and NO_x requires that the excess concentrations contain information about the same emissions. In order to derive coherent excess concentrations for NO_x and $ffCO_2$, allowing to determine local atmospheric $\frac{\Delta NO_x}{\Delta ffCO_2}$ concentration ratios, it is necessary to choose the same background boundary for both species. Otherwise, if the determined $ffCO_2$ excess concentrations are influenced by emissions from a larger area than the NO_x excess concentrations, the correlation between them would be generally weaker because of the heterogeneous spatial distribution of emissions, which would lead to a higher variability of $\frac{\Delta NO_x}{\Delta ffCO_2}$ ratios. The background boundary should therefore be close enough to the measurement station that, to a first approximation, NO_x removal from the atmosphere can be neglected (i.e. NO_x can be approximated to be transported as a conservative tracer). At the same time, to ensure a good signal-to-noise ratio, the background boundary should be far enough that the derived excess concentrations still contain most of the measured concentration signal. Thus, balancing these requirements, the location of the background boundary will depend on the NO_x lifetime and mean travel time to the station.

To differentiate between the excess concentrations in relation to MHD and in relation to the local background, the following nomenclature will be used: local excess concentrations are indicated by the symbol "Δ" preceding the species name, whereas excess concentrations relative to MHD are indicated by the abbreviation "ex." in the index. Equation 1 postulates that the measured concentration of a species (e.g. NO_x, CO_2 or $^{14}CO_2$) at the station (meas.) is composed of a concentration contri-

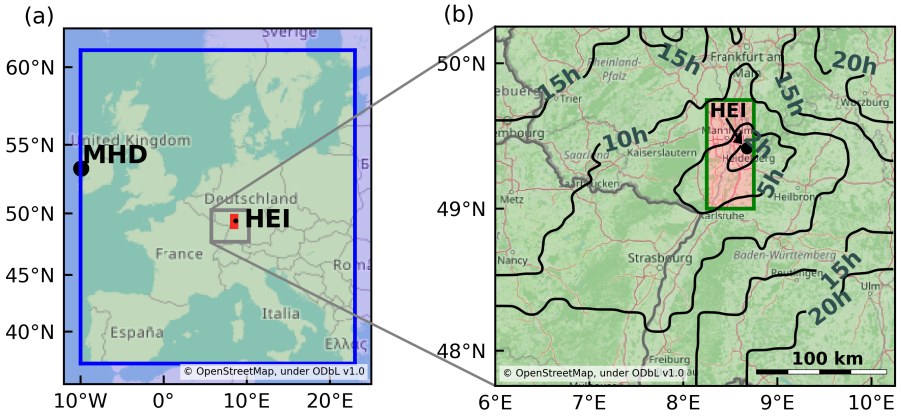

Figure 1. Division of the station catchment area into different domains, for the case of HEI, according to Eq. (1): European background $BG_{MHD/EU}$ (blue shaded area), contribution from the European domain $EU_{contr.}$ (green shaded area) and local domain $\Delta species$ (red shaded area). **(b)** The contour lines illustrate the mean simulated travel time of air masses to HEI for DJF 2019/20. The location of HEI and MHD is indicated.

bution from the European background $BG_{EU/MHD}$, a concentration contribution from the European domain $EU_{contr.}$, and a local concentration contribution $\Delta species$. Figure 1 illustrates the spatial division of the different domains for the case of Heidelberg.

$$meas. = BG_{EU/MHD} + EU_{contr.} + \Delta species = BG_{EU/MHD} + species_{ex.} \quad (1)$$

For NO_x we can expect the contribution from outside Europe to be 0 due to fast removal by atmospheric chemistry, and need only subtract the concentration contributions of the European domain from the measured NO_x concentrations to obtain ΔNO_x for the local domain, as shown in Eq. (2). For ^{14}C-based $ffCO_2$, as excess concentrations are derived relative to MHD ($ffCO_{2,\,ex.}$) (Maier et al., 2023), the local excess concentration can also be calculated by subtracting the concentration contributions from the European domain, as shown in Eq. (3).

$$\Delta NO_x = meas. - EU_{contr.} \quad (2)$$

$$\Delta ffCO_2 = ffCO_{2,ex.} - EU_{contr.} \quad (3)$$

Thus, in the context of this method only the contribution of the European domain needs to be determined to calculate local excess concentrations. Therefore, in the following, when we refer to the local background, this concerns the contribution from the European domain.

2.2.1 Setting the local background boundaries

The atmospheric chemistry of NO_x involves multiple different processes, with several reactions being dependent on solar radiation, temperature, and concentrations of ozone and radicals (see Kenagy et al. (2018) for an overview). These in turn depend on NO_x concentrations themselves, thus introducing feedback loops (Valin et al., 2013). Consequently, the lifetime

of NO_x varies considerably with the atmospheric conditions, resulting in significant spatial and temporal variations. Daytime lifetime estimates range from $2\,\mathrm{h}$ to $11\,\mathrm{h}$ in summer and $18\,\mathrm{h}$ to 2 days in winter (Martin et al., 2003; Liu et al., 2016; Romer et al., 2016; Kenagy et al., 2018). Lifetime estimates for Germany have been derived by Beirle et al. (2003) and Beirle (2004). From these, we assume typical NO_x lifetimes of $6\,\mathrm{h}$ for summer, $20\,\mathrm{h}$ for winter, and $16\,\mathrm{h}$ for the intermediate seasons, with an uncertainty of $\pm 2\mathrm{h}$ for the typical NO_x lifetimes, based on the range of estimates.

Figure 1 (b) illustrates the spatial distribution of simulated mean travel times to Heidelberg in the Rhine Valley for the winter months (DJF) of 2019/2020. These were simulated with the Stochastic Time-Inverted Lagrangian Transport (STILT) model, driven by meteorological fields from the Weather Research and Forecast (WRF) model (Nehrkorn et al., 2010) with a horizontal resolution of $2\,\mathrm{km}$. The WRF simulations are based on hourly, 0.25° resolution meteorological fields from the European Centre for Medium-Range Weather Forecast (ECMWF) Reanalysis v5 (ERA5; Hersbach et al. (2020)). The mean winter travel times already exceed $15\,\mathrm{h}$ or $20\,\mathrm{h}$ at distances of 100 to $200\,\mathrm{km}$. On this timescale, the majority of the emitted NO_x contribution from the European domain will not contribute significantly to the observations at the station due to its short atmospheric lifetime of a few hours to a day. Therefore, in most meteorological situations, the observed NO_x concentration only provides information on a close vicinity around the station.

For the determination of the location of the local background boundaries, the WRF-STILT model was used to calculate time-resolved (hourly) and gridded footprints (with a horizontal resolution of ca. $1\,\mathrm{km}$) for the HEI observation site within the Rhine Valley domain (47.75° N to 50.25° N and 6° E to 10.25° E indicated as grey rectangle in Fig. 1 (a)). These footprints describe the sensitivity of the HEI observation site on upwind surface fluxes within the Rhine Valley. They have been simulated by releasing 100 particles per hour from the Heidelberg site and calculating the particle trajectories backward in time. The footprints are mapped with high-resolution NO_x and $ffCO_2$ fluxes from the TNO inventory (Dellaert et al., 2019; Denier van der Gon et al., 2019) to get the NO_x (and $ffCO_2$) contribution from each grid cell. The simulations incorporate the most basic atmospheric NO_x chemistry through an exponential lifetime approach. The time-resolved and gridded footprints were multiplied by a factor $e^{-\frac{T}{\lambda}}$, where T is the travel time of the air mass and λ is the assumed atmospheric lifetime of NO_x, to describe the atmospheric decay of NO_x along the footprint.

Each grid cell contributes a specific share of the total simulated NO_x concentration for HEI, which depends on the emission of that grid cell, the sensitivity of the footprint to the grid cell, and the travel time from the grid cell to the station. This is referred to as the NO_x contribution of that grid cell, with the sum of all contributions being equal to the total simulated NO_x concentration. We analysed the spatial distribution of the NO_x contributions for HEI to identify a suitable location of the local background. For the mean simulated NO_x contributions shown in Fig. 2 (a) & (b), the NO_x contribution maps of the high-resolution domain were aggregated to a coarser resolution of 0.25°, which is used for simulating the European contributions (see Sect. 2.2.2).

The Heidelberg grid cell and the ones directly surrounding it have by far the highest NO_x contributions. Therefore, the boundary for the background was chosen as indicated by the green border in Fig. 2 (a) and (b) (49° N, 49.75° N, 8.25° E and 8.75° E), encompassing six grid cells next to Heidelberg to cover most NO_x contributions while still considering modest travel times. In summer (JJA) 86.1% of the simulated NO_x contributions from the Rhine Valley originate from within these

boundaries and in winter (DJF) 77.8%. Thus, the NO_x excess concentrations relative to this background still contain most of the measured signal. The domain defined by these boundaries will subsequently be referred to as the "local" domain and extends about 30 km to the West of HEI and about 40 km to the North and the South. The domain between these boundaries and the European background is referred to as the "European" domain.

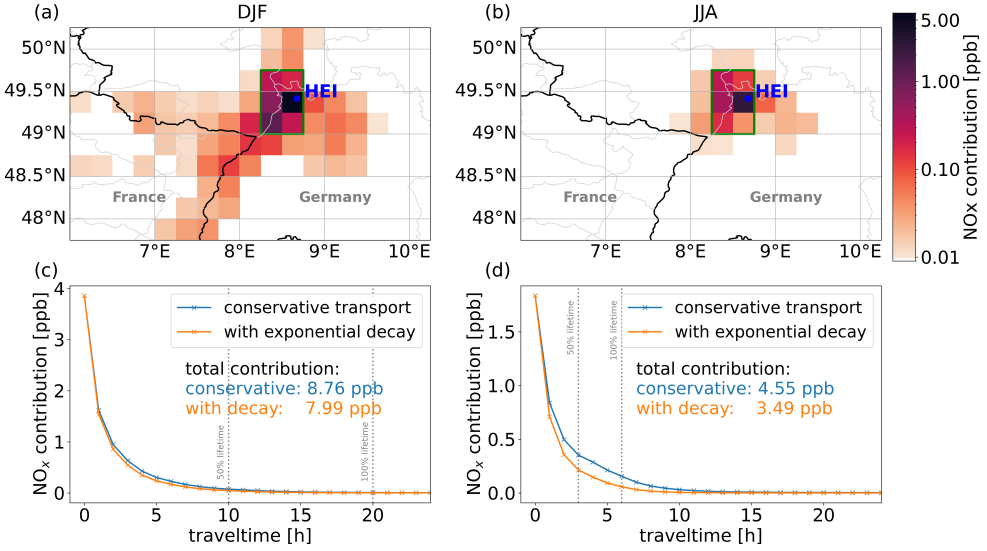

Figure 2. **(a)** Mean simulated NO_x contributions for winter and **(b)** summer months in 2020 on a 0.25° grid. The blue dot indicates the location of Heidelberg. The green rectangle shows the chosen boundary for the local background. **(c)** Simulated mean NO_x contributions from the local domain as a function of their travel time for winter and **(d)** summer months in 2020. The vertical dotted lines indicate 50% and 100% of the lifetime of NO_x, respectively. The results as for a conservative transport without decay are displayed in blue. The results obtained with the exponential decay applied are shown in orange.

To further investigate NO_x contributions with respect to the air mass travelling times within the local domain, Fig. 2 (c) and (d) show the winter and summer distributions of the mean NO_x contributions, with and without the exponential decay, based on simulations of the high-resolution model. For the winter months, 99.8% of the NO_x contributions have a travel time less than the typical NO_x winter lifetime and 98% have a travel time less than half of it. In the summer months, this is still true for 97.1% and 86.7% respectively. The difference between the NO_x concentrations simulated with and without the exponential decay shows that assuming conservative transport within the local domain introduces a bias on the order of 1 ppb (0.77 ppb for winter, 1.06 ppb for summer). The assumption of conservative transport leads to an underestimation of $\sim 10\%$ on the average winter NO_x signal of 8.76 ppb and a more significant underestimation of $\sim 25\%$ on the average summer signal of 4.55 ppb. For winter, the overall underestimation and travel times are small enough that the assumption of conservative transport is deemed

acceptable. For summer however, travel times are of the same order as the atmospheric lifetime, resulting in a significant underestimation. The effects of this are discussed in Sect. 2.3.

2.2.2 Determination of the local background concentrations

To calculate the local background concentrations, the STILT model was driven with coarser, 0.25° resolution meteorological fields from the ECMWF Integrated Forecasting System (IFS). Again, 100 particles were released each hour from the HEI site and their back-trajectories were calculated for 10 days or until they left the European model domain (32° N to 74° N, 16° W to 36° E). The resulting footprints are mapped with European NO_x and $ffCO_2$ emissions from TNO, but with the emissions inside the local domain set to 0, so that only emissions from the European domain were propagated to the HEI station. Due to the seasonal change in NO_x lifetime, the model was run three times with NO_x lifetimes of 6, 16, and 20 h to produce hourly resolved background concentrations for summer, spring/autumn, and winter respectively. Season changes were assigned based on the temperatures observed at the station: months with mean temperatures below 10°C were assigned as winter, months with over 19°C as summer, and the remaining months as spring/autumn.

Previous studies revealed that the STILT and TNO modelling framework shows a remarkable capability to model synoptic concentration changes for HEI station (Maier et al., 2022). However, the STILT model and the TNO emission inventory are imperfect and subject to uncertainties, thus the timing and the absolute value of the modelled local background concentrations should not be considered accurate on the hourly timescale. Thus, a rolling Gaussian smooth was applied on the modelled local background concentrations with a window size of 24 h and standard deviation of 3 h.

Figure 3 displays an example week, showing the modelled local background concentration time series, i.e. the contribution from the European domain and the measured concentrations for $ffCO_2$ and NO_x. The modelled local background concentrations are predominantly lower than the measured concentrations. Comparing the two shows different situations with varying influence from the local domain (excess between measured data and local background). In a few cases the simulated background concentrations do exceed the real measurements, resulting in negative local excess concentrations, but only for 1.7%, with only 0.1% outside a 1σ range from 0 ppb. The average simulated contributions from the European domain for 2020 and 2021 were 1.49 ppb for NO_x and 2.93 ppm for $ffCO_2$, with standard deviations of 1.5 ppb and 2.8 ppm respectively. This corresponds on average to approximately 10% of the total measured NO_x concentration and 25% of the $ffCO_{2,\,ex.}$ concentration calculated from $^{14}CO_2$ measurements.

2.2.3 Assessing the uncertainty of the local background concentrations

The additional uncertainty related to the modelled local background concentration can be separated into three main contributions: the uncertainties of the emissions from the TNO inventory, the errors of the transport model, and the uncertainty of the lifetimes used in the exponential decay.

The uncertainties of the emissions from the TNO inventory were approximated as 40% for $ffCO_2$ and 45% for NO_x, based on the uncertainties of the national emissions and their spatial distribution (I. Super, personal communication, based on Super et al. (2024)). Since a relative change of the emissions propagates linearly through the transport model, these relative uncertainties

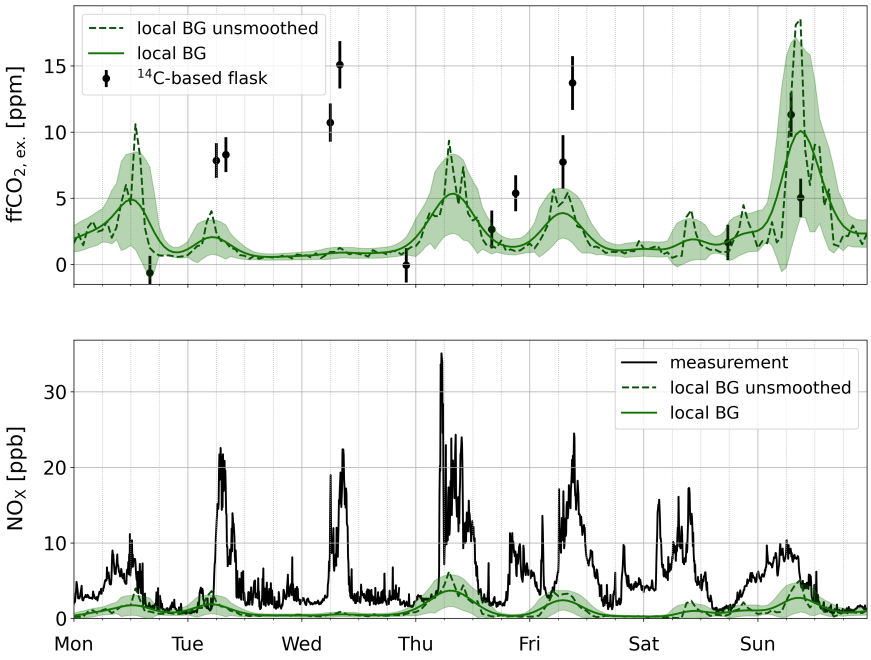

Figure 3. Measured concentrations (in black) and simulated background (in dashed green) from 13.04.2020 until 19.04.2020 for Heidelberg station. The solid green curve shows the background concentrations after the Gaussian smooth, with its 1σ confidence interval according to the combined uncertainties from emission-, model transport- and lifetime-uncertainties. Please refer to main text for a detailed explanation.

were directly applied to the simulated background to calculate the corresponding emission-related uncertainty. The actual impact on the uncertainty of the simulated concentrations is probably smaller due to the random errors from the grid cells compensating each other. As we want to make a conservative estimation of the uncertainty, we choose to use the greater value as an upper boundary.

As an approximation for the errors of the transport model and their impact on the simulated background, the main factor was assumed to be temporal misalignment of the simulated and "true" background. The standard deviation of the unsmoothed data over a $6\ \mathrm{h}$ window was used to assess the possible impact of such a shift and to estimate the corresponding uncertainty. The median of this background uncertainty is about 30% for the modelled NO_x and $ffCO_2$ concentrations. This time-dependent estimate of transport uncertainty has the advantage of yielding higher uncertainties for periods with strong fluctuations in the simulated concentrations, mirroring the limited reliability of the simulated background concentrations. When averaging over longer periods, the temporal misalignment should average out. This contribution to the background uncertainty is therefore mainly important when looking at individual hours.

To assess the impact of the NO_x lifetime uncertainties on the NO_x background, the modelled background concentration B at a certain hour can be regarded as a "mean" air mass with some initial concentration E and a travel time T. The dependency of the background concentration B on the lifetime λ can then directly be described by Eq. 4, where c is the contribution with

a travel time of 0 h.

$$B = E * \exp(-T/\lambda) + c \quad (4)$$

As the background was simulated for 6, 16, and 20 h lifetimes (and additionally for 18 h and 24 h), the unknown parameters E, T and c can be determined analytically. The lifetime-dependent change in the modelled NO_x concentration can thus be calculated analytically, without running the model. For the assumed uncertainty of 2 h of the seasonally dependent lifetime this yields a lifetime-related background uncertainty of 40% for 6 h, 11% for 16 h, and 7% for 20 h lifetime.

Assuming the three uncertainty components are independent, the resulting uncertainties for the simulated background concentrations are on average about 60% for NO_x and 50% for $ffCO_2$. They are shown as shaded uncertainty range of the modelled local background concentrations in Fig. 3. The uncertainty analysis of the modelled background concentrations conducted here is incomplete. It could be enhanced through an ensemble approach, utilising alternative transport models, meteorological driver data, and emission inventories. However, this is beyond the scope and intention of this exploratory work. We acknowledge the inherent limitation of using modelled local background concentrations, while recalling that these account for only 10% of the measured NO_x and 25% of the $ffCO_2$ signals.

2.3 Construction of a ΔNO_x-based $\Delta ffCO_2$ record

To construct continuos hourly ΔNO_x-based $\Delta ffCO_2$ estimates, the hourly ΔNO_x record is divided by an average atmospheric $\frac{\Delta NO_x}{\Delta ffCO_2}$ ratio. The local excess concentrations ΔNO_x and $\Delta ffCO_2$ are determined with respect to the simulated local background concentration according to Eq. (2) and (3). For each $^{14}CO_2$ flask analysis we calculated a $ffCO_{2,\,ex.}$ concentration relative to a marine $^{14}CO_2$ background record from MHD using Eq. (3) from Maier et al. (2023), which includes corrections for ^{14}C contamination from nuclear facilities and biospheric respiration. Please refer to Maier et al. (2023) for more details and for the construction of the marine $^{14}CO_2$ background. Following Maier et al. (2024a), a weighted total least-squares regression was applied to determine mean atmospheric $\frac{\Delta NO_x}{\Delta ffCO_2}$ ratios.

By design, this method is insensitive to systematic shifts and scaling in the determination of ΔNO_x, as long as the sampled flasks are representative of the conditions at the station. This is because such systematic biases affect the determination of the $\frac{\Delta NO_x}{\Delta ffCO_2}$ ratio and the continuous ΔNO_x record on which the ratio is applied in the same way, and therefore cancel each other out in the calculation of the ΔNO_x-based $\Delta ffCO_2$ estimates. However, the statistical variability around a mean bias still has an effect. A mean bias is corrected for by the method, as described above, but the variability of that bias results in an effectively higher variability in the observed $\frac{\Delta NO_x}{\Delta ffCO_2}$ ratios and therefore a higher uncertainty in the ΔNO_x-based $\Delta ffCO_2$ estimates. This would be, for example, a mean bias caused by NO_x removal from the atmosphere in the local domain, with variability due to the variability of atmospheric conditions leading to different levels of removal.

Returning to the underestimation of ΔNO_x in the summer months due to significant removal of NO_x from the atmosphere within the local domain (see Sect. 2.2.1), the mean bias caused by this underestimation has no effect on the estimation of $\Delta ffCO_2$ as just stated. However, the variability of the underestimation increases the uncertainty of the derived ratio and $\Delta ffCO_2$ concentrations. From the concentration contributions simulated with the high resolution model, we estimated this additional

uncertainty for the $\Delta ffCO_2$ estimates at approximately $0.4\ \mathrm{ppm}$ using a Monte Carlo approach. Given that this is much lower than the typical $1.5\ \mathrm{ppm}$ uncertainty of ^{14}C-based $\Delta ffCO_2$ estimates, the choice of background is still deemed appropriate for the summer months, although a higher uncertainty for the ΔNO_x-based estimates is to be expected. For winter, we recall that the underestimation was much smaller, and therefore the impact is smaller still than for summer.

3 Results

3.1 ΔNO_x / $\Delta ffCO_2$ ratios from flask samples

Figure 4 (a) shows the local ΔNO_x enhancements against the ^{14}C-based local $\Delta ffCO_2$ enhancements. The flask samples were collected under a range of different atmospheric conditions and at different times of the day to be representative of the mix of conditions encountered at the station. While there are some very small or negative and some very high ratios, most ratios fall within the expected range for a mix of traffic and heating emissions for Heidelberg (shown by the blue and green lines in the figure). Scatter plots for winter and summer separately can be found in Fig. A1. For winter the flasks fall within the expected range for a mix of traffic and heating. For summer the flasks mostly fall in the expected range for traffic emissions and show lower excess concentrations than in winter. Flasks with a ratio uncertainty of over 100% were excluded from the determination of the mean $\frac{\Delta NO_x}{\Delta ffCO_2}$ ratio (but included in the determination of the uncertainty of the resulting ΔNO_x-based $\Delta ffCO_2$ estimates). As outlined in Maier et al. (2024a), an error-weighted regression through the data was used to obtain unbiased estimates of the mean atmospheric $\frac{\Delta NO_x}{\Delta ffCO_2}$ ratios.

The regression over all the flasks collected in 2020 and 2021 yields an average ratio of $1.49 \pm 0.04\ \mathrm{ppb\,ppm^{-1}}$, with an R^2 value of 0.84. Due to the temporal changes in atmospheric chemistry and the mix of emissions, a seasonal and diurnal cycle of the atmospheric $\frac{\Delta NO_x}{\Delta ffCO_2}$ ratio is expected. In Fig. 5 monthly and hourly derived atmospheric $\frac{\Delta NO_x}{\Delta ffCO_2}$ ratios are shown. The seasonal and diurnal cycle are qualitatively similar to what would be expected from the inventory, with a higher ratio in summer than in winter, following the heating cycle and two peaks in the morning and evening because of rush hour traffic. The monthly atmospheric $\frac{\Delta NO_x}{\Delta ffCO_2}$ ratios clearly indicate two different ratios for winter (October to April) and summer (May to September). For all winter samples, the regression yields an average atmospheric $\frac{\Delta NO_x}{\Delta ffCO_2}$ ratio of $1.40 \pm 0.04\ \mathrm{ppb\,ppm^{-1}}$ with an R^2 value of 0.86, while for all summer samples a higher ratio of $2.12 \pm 0.13\ \mathrm{ppb\,ppm^{-1}}$ with an R^2 value of 0.55 is found. The weaker correlation for the summer flasks is related to the overall smaller signal strength; if for the winter period only flasks in the same concentration range as the summer period ($\Delta ffCO_2 < 19\ \mathrm{ppm}$) would be used, the R^2 value would drop to 0.63.

Dividing the samples into summer and winter retains a sufficient number of samples per season, ensuring the regression remains resilient against non-representative ratios obtained from single flasks. However, if only a small number of flasks are available, for example in June where only background conditions were sampled or for specific hours of the day, the regression can be heavily biased by a single observation with a non-representative ratio (see Fig. 5). Therefore, we refrained from deducing a diurnal cycle even though a certain structure is visible.

The data was also analysed for any dependency on wind direction and speed, but no relevant correlation was found.

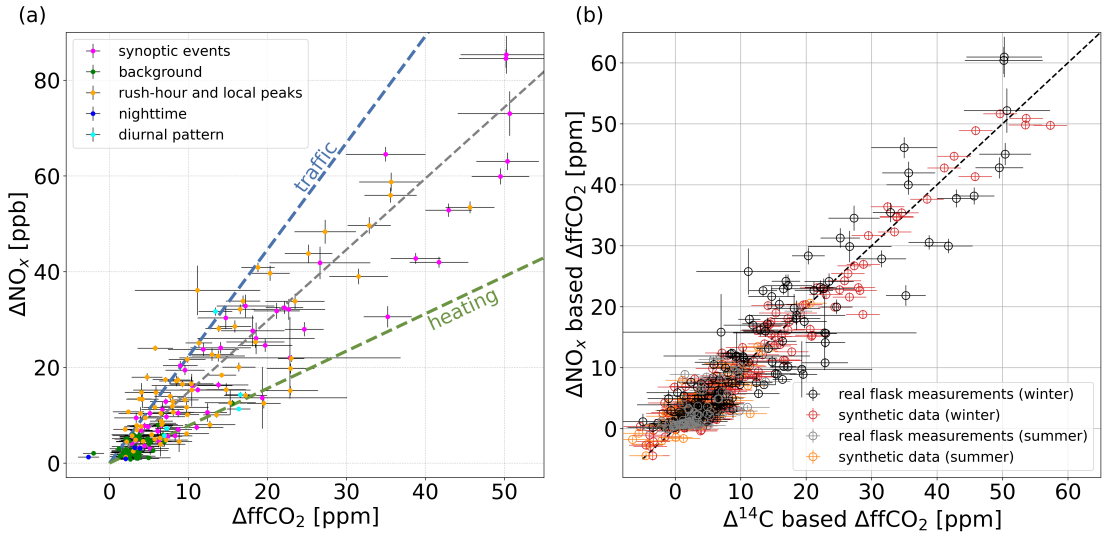

Figure 4. (a) Scatter plot of the local ΔNO_x and $\Delta ffCO_2$ concentrations for all valid flask measurements. The colour of each data point indicates the sampling situation. The dashed grey line represents the weighted total least-squares regression line. The blue and green lines show the average TNO inventory emission ratios for the traffic and heating sector in the vicinity of Heidelberg. **(b)** Comparison between ΔNO_x- and ^{14}C-based local $\Delta ffCO_2$ concentrations for the summer (grey circles) and winter (black circles) flasks. Synthetic data (red circles for winter data and orange circles for summer data) was generated by assuming a constant summer and winter ratio respectively.

3.2 Uncertainty of the ΔNO_x-based $\Delta ffCO_2$ record

Following Maier et al. (2024a), the uncertainty of the ΔNO_x-based $\Delta ffCO_2$ estimates was estimated by comparison to the ^{14}C-based $\Delta ffCO_2$ estimates (see Fig. 4 (b)). A regression through this data unsurprisingly results in a slope of 1, as the flask were used to derive the average summer and winter ratios. The distribution of the ΔNO_x-based $\Delta ffCO_2$ estimates around the 1:1 line is caused by the uncertainties of the measurements and the background estimation, as well as the neglected spatio-temporal variability of the atmospheric $\frac{\Delta NO_x}{\Delta ffCO_2}$ ratios on sub-seasonal time scales. The root-mean-square-deviation (RMSD) between the ΔNO_x- and ^{14}C-based $\Delta ffCO_2$ can be used to estimate the uncertainty of the ΔNO_x-based $\Delta ffCO_2$ record. As the RMSD is dependent on the range of $\Delta ffCO_2$ concentrations, the normalised RMSD (NRMSD) was calculated by dividing the RMSD by the mean ^{14}C-based $\Delta ffCO_2$ concentrations. The (N)RMSD over all flasks is 3.94 ppm (46%), while it is 4.45 ppm (41%) for the winter period and 2.46 ppm (73%) for the summer period.

In order to assess which share of this uncertainty can be attributed to the measurement and background uncertainties and how much is due to the neglected variability of the $\frac{\Delta NO_x}{\Delta ffCO_2}$ ratios, a synthetic data experiment was performed analogue to the procedure in Maier et al. (2024a). With this, an uncertainty of 2.65 ppm (31%) over all flasks and 3.00 ppm (28%) or 1.93 ppm (57%) for the winter or summer periods, respectively, can be attributed to the measurement and background uncertainties. Assuming these to be independent of the ratio variability, the uncertainty of the $\Delta ffCO_2$ concentrations due to the

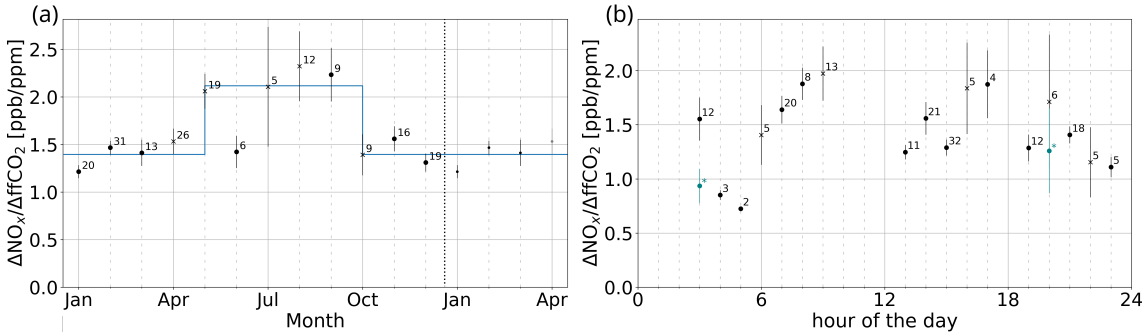

Figure 5. (a) Seasonal cycle with ratios calculated by separate regression for each month. The number next to each data point indicates the number of measurements in that month. Values denoted by a cross instead of a circle have an associated R^2 value of less than 0.5. The blue line illustrates the ratios calculated by two regressions over a summer period from May to September, and a winter period from October to April. **(b)** Diurnal cycle with ratios calculated by separate regression for each hour of the day. The number indicates the number of measurements in that hour. Values denoted by a cross instead of a circle have an associated R^2 value of less than 0.5. For three hours there is only one flask available, these were therefore excluded from this analysis. For hours 3 and 20 there is a second value shown with a teal coloured circle representing an alternative ratio under exclusion of three flasks from a single synoptic event for hour 3 and one traffic-signal flask for hour 20.

ratio variability can be estimated through Gaussian error propagation. An uncertainty of $2.91\ \mathrm{ppm}$ (34%) over all flasks can therefore be attributed to the ratio variability. This results in an uncertainty of $3.29\ \mathrm{ppm}$ (30%) in winter and $1.52\ \mathrm{ppm}$ (45%) in summer.

3.3 Comparison with $CO_{ex.}$- and ^{14}C-based $ffCO_{2,ex.}$ records

We compared the constructed ΔNO_x-based $\Delta ffCO_2$ record with a ^{14}C-based $ffCO_{2,ex.}$ record from fortnightly integrated radiocarbon samples and a $CO_{ex.}$-based $ffCO_{2,ex.}$ record to investigate the similarities and differences between the records. Note that the ratio for CO was determined by Maier et al. (2024a) for the years 2019 and 2020 and applied here for the years 2020 and 2021. The integrated radiocarbon samples are completely independent of the flask measurements used to derive the $\Delta NO_x/\Delta ffCO_2$ ratio and therefore allow for a meaningful evaluation of the ΔNO_x-based estimates.

Maier et al. (2024a) estimated an uncertainty of $3.95\ \mathrm{ppm}$ (39%) for the $CO_{ex.}$-based $ffCO_{2,ex.}$ estimates and attributed $2.07\ \mathrm{ppm}$ (20%) to the background and measurement uncertainty. Consequently, an uncertainty of $3.36\ \mathrm{ppm}$ (33%) can be attributed to the $\frac{CO_{ex.}}{ffCO_{2,ex.}}$ ratio variability. While the background and measurement uncertainty for the $CO_{ex.}$-based record is smaller than for the ΔNO_x-based record (even without considering the additional uncertainty of the European domain $ffCO_2$ contribution), the relative uncertainty due to the ratio variability is almost identical for both proxies, although for CO no seasonally varying ratio was applied.

Figure 6 shows a comparison of monthly $ffCO_{2,ex.}$ means for the years 2020 and 2021. The local ΔNO_x-based $\Delta ffCO_2$ estimates and the $ffCO_2$ contribution from the European domain are shown as blue and grey columns, which when stacked

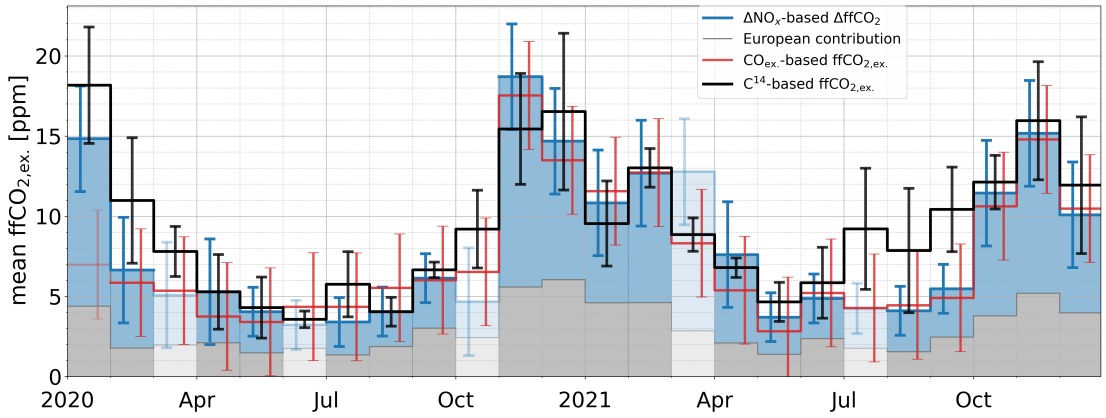

Figure 6. Mean monthly $ffCO_{2,ex.}$ concentration estimates for Heidelberg estimated through independent proxies. The grey bars give the $ffCO_2$ contribution from the European domain (see Sect. 2.2). Stacked upon this, the ΔNO_x-based $\Delta ffCO_2$ concentrations are shown in blue. The total height of this column represents the ΔNO_x-based $ffCO_{2,ex.}$ estimate relative to MHD. The blue error bars for ΔNO_x-based $ffCO_{2,ex.}$ report the uncertainty of the excess concentration relative to MHD, including the uncertainty of the $ffCO_2$ background. Mean monthly ^{14}C-based $ffCO_{2,ex.}$ concentrations based on fortnightly integrated ^{14}C samples are shown in black with their uncertainties. These were calculated by averaging the $ffCO_{2,ex.}$ from the day and night time integrated ^{14}C samples (calculated according to the methods described in Maier et al. (2023)), assuming that they represent the day and night halves of the day respectively. $CO_{ex.}$-based $ffCO_{2,ex.}$ relative to MHD is shown in red with the uncertainty of 3.95 ppm estimated by Maier et al. (2024a). Periods with low data coverage are indicated in transparent. In January 2020, the CO data coverage is only 15%. For NO_x, the data coverage is low in March (63%), June (42%) and October (16%) 2020, as well as March (46%) and July (18%) 2021.

together give the composite ΔNO_x-based $ffCO_{2,ex.}$ estimates relative to MHD. The $CO_{ex.}$- and ^{14}C-based estimates are shown as red and black lines, respectively. The monthly mean ΔNO_x-based $ffCO_{2,ex.}$ concentrations are on average about 0.6 ppm higher than the $CO_{ex.}$-based estimates and 1.1 ppm lower than the ^{14}C-based. The ΔNO_x- and $CO_{ex.}$-based monthly mean $ffCO_{2,ex.}$ concentrations generally show a good agreement with each other and with the $ffCO_{2,ex.}$ concentrations from the integrated samples. A majority of the higher differences between the records are in months with low data coverage of one proxy and are overall well within the uncertainties of the records. A more notable discrepancy is observed between the integrated samples and the proxy based records for the months of July through September 2021, which should warrant further investigation into the reasons for this, but is beyond the scope of this study.

Two example weeks of proxy-based $ffCO_{2,ex.}$ estimates are shown in Fig. 7 to further compare the ΔNO_x- and $CO_{ex.}$-based records. The ^{14}C-based flask estimates generally agree well with the proxy-based estimates. On average, the $CO_{ex.}$-based estimates are 0.3 ppm lower than the ΔNO_x-based. The ΔNO_x-based estimates for the rush hour peaks are mostly higher than for the $CO_{ex.}$-based which is often corroborated by the ^{14}C-based estimates. On multiple occasions the $CO_{ex.}$ and ^{14}C-based $ffCO_{2,ex.}$ records reach lower than the ΔNO_x-based record, partly below the modelled contribution from the local background.

Figure 7 (b) shows a contrasting situation at the end of the week with prevailing winds from the east where the $CO_{ex.}$-based estimates are substantially higher compared to the ΔNO_x- and ^{14}C-based. As the $CO_{ex.}$-based record uses smoothed MHD measurements as background for CO, in the minority of cases where air masses are not originating from the Atlantic, this can lead to an over- or understated background, as illustrated here. At the same time, the constructed local background uses a smoothed version of the modelled data, averaging out minima and high peaks. The determination of the $\frac{\Delta NO_x}{\Delta ffCO_2}$ ratio accounts for this on some scale, as it uses the same background. Still, in situations that are not well represented by the available flasks, this can have a relevant impact. For example, on the 13 April 2020 (Fig. 7 (a), Monday), a background problem is obvious, whereby the composite ΔNO_x-based $ffCO_{2,ex.}$ estimate is substantially higher than the $CO_{ex.}$- and ^{14}C-based estimates. While the problems of both backgrounds are reflected in their uncertainties, this needs to be considered when analysing individual events.

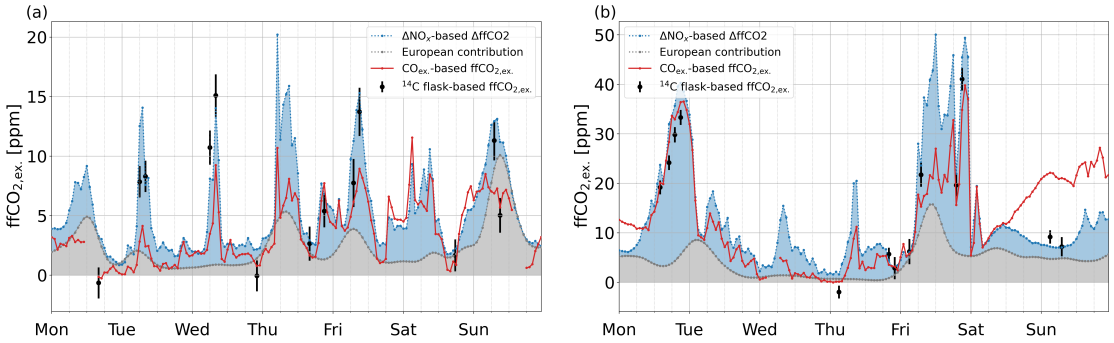

Figure 7. Example weeks of proxy based $ffCO_{2,ex.}$ records. $CO_{ex.}$-based excess $ffCO_2$ relative to MHD is shown in red. The grey bars give the $ffCO_2$ contribution from the European domain. Stacked upon this, the ΔNO_x-based $\Delta ffCO_2$ concentrations are shown in blue. The total height of this column represents the ΔNO_x-based $ffCO_{2,ex.}$ estimate relative to MHD. Additionally, the black data points show ^{14}C-based $ffCO_{2,ex.}$ estimates from flasks. (a) 13.04.2020 - 19.04.2020, (b) 01.02.2021 - 07.02.2021. Note that (a) and (b) have different y scales.

4 Discussion

The co-emission of NO_x and $ffCO_2$ makes ΔNO_x a potential proxy for continuous $\Delta ffCO_2$ estimates. The feasibility of such an approach in an urban environment, acknowledging the challenges involved, is demonstrated in our study. The comparison to two independent $ffCO_{2,ex.}$ records shows in general a good agreement with the ΔNO_x-based estimates and validates this approach for the example of Heidelberg. In the following, we critically discuss the benefits and challenges of ΔNO_x-based $\Delta ffCO_2$ estimation.

4.1 Challenges of a ΔNO_x-based proxy approach

The key challenges of the method lie in determination of coherent NO_x and $ffCO_2$ excess concentration, i.e. in the determination of an appropriate background, and the robust determination of atmospheric $\frac{\Delta NO_x}{\Delta ffCO_2}$ ratios with their seasonal and diurnal cycles.

The relatively short atmospheric lifetime of NO_x means that the observed NO_x concentrations provide information only about the immediate vicinity of the observation station. To utilise the correlation of NO_x and $ffCO_2$, it is crucial to ensure that the observed NO_x and $ffCO_2$ signals pertain to the same catchment area. Therefore, determining an appropriate common local NO_x and $ffCO_2$ background is important for the quantitative use of ΔNO_x-based $\Delta ffCO_2$ estimates. In an urban context, this would ideally be accomplished by a measurement network with up- and downwind measurements of $^{14}CO_2$ and NO_x, allowing direct, measurement-based calculation of excess concentrations. As such a network was not available in the case of Heidelberg, the STILT model and TNO emission inventory were used to simulate background concentrations for a region of about $40\,\mathrm{km}$ x $80\,\mathrm{km}$ around Heidelberg. This required the consideration of the short atmospheric lifetime of NO_x, which was taken into account through a very simplistic exponential decay approach, with different lifetimes for each season. Consequently, this model approach introduced additional uncertainties through the uncertainties of the emission inventory, the transport model, and the lifetimes used for the exponential decay of NO_x. This is reflected in the higher background uncertainties of 40% for NO_x and 30% for $ffCO_2$. As described in Sect. 2.3, the choice of the background per se is not as crucial with regard to its absolute value, because the method used intrinsically accounts for shifts and scaling of the background. However, it is crucial for limiting the analysis to a region where the atmospheric chemistry of NO_x still allows for an adequate observation of the correlation between ΔNO_x and $\Delta ffCO_2$, which is necessary to obtain low uncertainties. The employment of the most simplified approach of directly using the European $ffCO_{2,ex.}$ estimates and the measured NO_x signal without background correction would result in the uncertainty of the ΔNO_x-based $\Delta ffCO_2$ estimates increasing by about $1\,\mathrm{ppm}$. Given that the estimated uncertainties of the ΔNO_x-based $\Delta ffCO_2$ estimates are comparable to those of the $CO_{ex.}$-based estimates, we conclude that our described approach to the choice of background was adequate.

The atmospheric $\frac{\Delta NO_x}{\Delta ffCO_2}$ ratios are influenced by the atmospheric chemistry of NO_x and the changing shares of emission sectors due to their different emission ratios. This leads to distinct seasonal and diurnal cycles in the atmospheric $\frac{\Delta NO_x}{\Delta ffCO_2}$ ratios (see Fig. 5). The observed cycles generally agree qualitatively with the emission ratios from the inventory. However, we found that for lower numbers of available flasks, average ratios for individual months or hours can be highly influenced by individual flasks and are not necessarily representative, especially in summer. Therefore, only two different ratios for summer at $2.12 \pm 0.13\,\mathrm{ppb\,ppm^{-1}}$ and winter at $1.40 \pm 0.04\,\mathrm{ppb\,ppm^{-1}}$ were applied for the estimation of ΔNO_x-based $\Delta ffCO_2$. The seasonal means are primarily influenced from samples collected during the afternoon and rush-hour times, as more flasks were sampled during these times and these flasks generally measured the highest excess concentrations, making them representative of periods most accurately captured by atmospheric transport models.

In particular, the neglected diurnal ratio variability should be further investigated, as this is one of the major sources for the overall uncertainty of the ΔNO_x-based $\Delta ffCO_2$ record. One possible approach which we tested, would be to take the basic shape of the diurnal cycle from the inventory and fit this to the observed ratios for the individual hours. However, applying

this method actually increased the uncertainty of the ΔNO_x-based $\Delta ffCO_2$ estimates by 50% to 6 ppm. This is not entirely surprising, considering that the inventory describes emission ratios, whereas our method requires mean atmospheric ratios. The difference between these is non trivial, especially at night and in the morning, as this depends on atmospheric conditions and the dynamics of the planetary boundary layer. By restricting this approach to afternoon hours only (11:00 to 16:00), a 2% improvement in the uncertainty can be achieved. Just restricting the original analysis to the afternoon and deriving a mean afternoon ratio already leads to a 3% improvement in the uncertainty. Consequently, a better quantitative determination of the diurnal cycle requires either more radiocarbon measurements for ratio determination, or an advanced atmospheric model to translate the inventory emission ratios into atmospheric concentration ratios, provided that the shape of the diurnal cycle from the inventory is correct.

The summer samples show a lower correlation between ΔNO_x and $\Delta ffCO_2$, as well as considerably higher relative uncertainties than the winter. This reflects the lower signal strength in summer and the higher variability due to the shorter atmospheric NO_x lifetime compared to winter. Overall, the method is therefore in general strongest on a winter afternoon and much more limited in its significance in summer.

Determining robust $\frac{\Delta NO_x}{\Delta ffCO_2}$ ratios also requires a representative data set on which the ratios are determined. The typical range of the continuous ΔNO_x-based $\Delta ffCO_2$ estimates (0–20 ppm) is lower than that of the ^{14}C-based flask estimates (2–35 ppm), suggesting that the flasks used to derive the $\frac{\Delta NO_x}{\Delta ffCO_2}$ ratio are not necessarily representative of the complete record. This originates from a sampling bias of the flask samples, which were disproportionately sampled during situations with high $ffCO_2$ concentrations and during daytime. In light of the uncertainties of the ^{14}C-based $\Delta ffCO_2$ estimates and the analysis costs, this is still a reasonable sampling approach. However, this should be kept in mind when using and interpreting the ΔNO_x-based $\Delta ffCO_2$ record.

4.2 Benefits of a ΔNO_x-based proxy approach

Despite all these challenges, the ΔNO_x and ^{14}C-based $\Delta ffCO_2$ concentrations show a strong correlation, with R^2 values of 0.86 in winter and still 0.55 in summer. This allows the determination of robust seasonal ratios with relatively small uncertainties. When combined with a more advanced transport and chemistry model, they can provide valuable information for validating emission inventories.

A main cause of the challenges, the short atmospheric lifetime of NO_x, is also a reason for a benefit of using ΔNO_x as a $\Delta ffCO_2$ proxy due to the local nature of the NO_x signal. The ΔNO_x-based $\Delta ffCO_2$ record relative to the local background combined with the $CO_{ex.}$-based $ffCO_{2,ex.}$ record relative to MHD allow the calculation of the local share of $ffCO_2$. As a result of the way in which the $\frac{\Delta NO_x}{\Delta ffCO_2}$ ratio is determined, the distribution of $ffCO_2$ into the local signal and background is calibrated by the flasks used for determining the ratio. Consequently, it is largely influenced by the local $ffCO_2$ background. In a scenario where a more complex and precise background with sparse temporal resolution is used, e.g. a measured ^{14}C-based $ffCO_2$ background or a highly complex model that is only evaluated for the sample times of the flasks, the above introduced simpler method can be used to effectively upscale the background and determine the local share of $ffCO_2$ on a high temporal resolution.

Furthermore, the comparison of the ΔNO_x- and $CO_{ex.}$-based records showed that while they generally produce similar records, there are also distinctly different structures for individual events. Where the two proxies show differing $ffCO_{2,ex.}$, no single proxy systematically agrees better with the ^{14}C-based flask data, highlighting that the two records offer distinct and complementary information. This calls for further studies on inverse modelling of $ffCO_2$ emissions with multiple proxies, leveraging the different sensitivities of the proxies to the near and far field and to different emission sectors. This in turn opens up opportunities for spatial and sectoral attribution of emissions.

5 Conclusions

ΔNO_x shows considerable potential as a proxy for $\Delta ffCO_2$ in an urban context, as shown here for the case of Heidelberg. Even with a simple approach to account for its atmospheric chemistry and ratio variability, a strong correlation between ΔNO_x and $\Delta ffCO_2$ is observed, allowing the construction of a high temporal resolution ΔNO_x-based $\Delta ffCO_2$ record with uncertainties comparable to the use of CO as a proxy.

For this, a local background was modelled with the STILT model and TNO emission inventory to derive coherent ΔNO_x and $\Delta ffCO_2$ excess concentrations. Two different ratios for summer at $2.12 \pm 0.13\ \mathrm{ppb\,ppm^{-1}}$ and winter at $1.40 \pm 0.04\ \mathrm{ppb\,ppm^{-1}}$ were obtained through an error-weighted regression and applied to a continuous ΔNO_x record for the estimation of ΔNO_x-based $\Delta ffCO_2$. A comparison with the ^{14}C-based $\Delta ffCO_2$ from the flasks was used to estimate the uncertainty of the ΔNO_x-based estimates at about $4\ \mathrm{ppm}$. Approximately $2.6\ \mathrm{ppm}$ could be attributed to the measurement and background uncertainties, while about $3\ \mathrm{ppm}$ were attributed to the ratio variability. This is comparable with the uncertainties for $CO_{ex.}$-based estimates in Heidelberg (Maier et al., 2024a). Moreover, the ΔNO_x-based estimates are overall in good agreement with independent $CO_{ex.}$- and fortnightly ^{14}C-based estimates. Concurrently, they display distinctive structures that indicate a potential information gain from incorporating a ΔNO_x-based record into model simulations. The extent to which the method can be applied to other (also potentially non urban) stations represents an exciting avenue for further research, though the results from this study indicate a high potential for the application in urban measurement networks.

One of the key challenges of the method is the short atmospheric lifetime of NO_x. This mandates the careful identification of an appropriate common background to determine the excess concentrations of NO_x and $ffCO_2$. The pronounced seasonal and diurnal cycle of atmospheric $\frac{\Delta NO_x}{\Delta ffCO_2}$ ratios necessitates a representative and comprehensive set of flask measurements to ensure its accurate and robust determination. As a consequence, the summer months present a particularly challenging period, given that the lifetime is shortest at this time and the predominantly low signals result in a less favourable signal-to-noise ratio. Urban measurement networks with up- and downwind sampling of $^{14}CO_2$ and NO_x provide the ideal setup to accommodate these challenges through direct background measurements and short travel times over the city.

In turn, when these challenges are adequately addressed, the short lifetime of NO_x can also provide benefits, such as insights into the local share of $ffCO_2$. In conclusion, while this work highlights the potential of constructing proxy based $\Delta ffCO_2$ records, it also reiterates the importance of systematic ^{14}C measurements to provide the necessary constraints on the changing ratios between the proxies and $ffCO_2$.

Data availability. The flask results and NOx data from Heidelberg, as well as the modelled local backgrounds can be found in Juchem et al. (2025, https://doi.org/10.11588/DATA/KI8DTQ).

Appendix A: ΔNO_x and $\Delta ffCO_2$ for winter and summer flasks

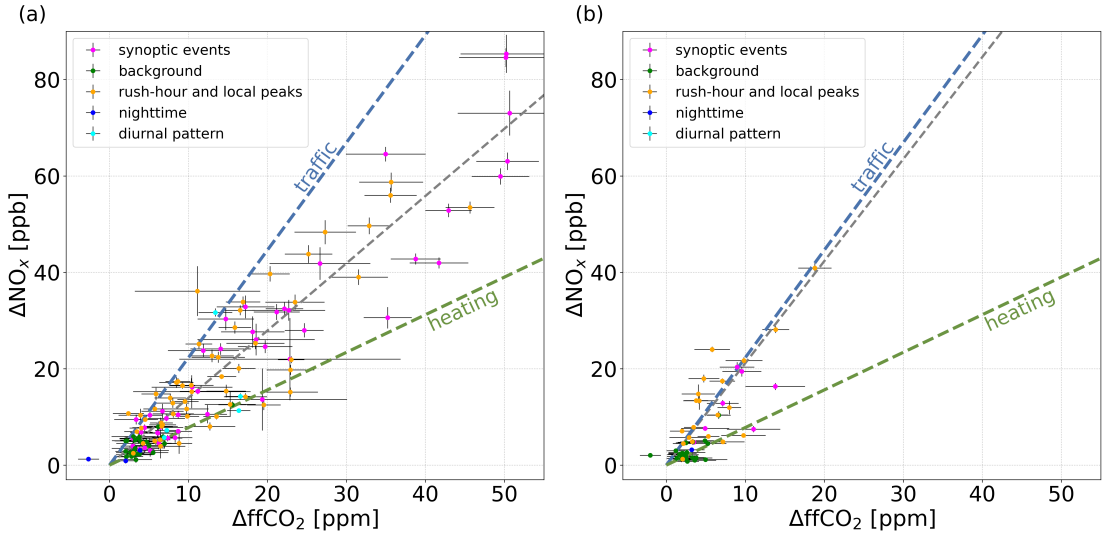

Figure A1. Scatter plot of the local ΔNO_x and $\Delta ffCO_2$ concentrations for all valid flask measurements in **(a)** winter (October to April) and **(b)** summer (May to September). The colour of each data point indicates the sampling situation. The dashed grey line represents the weighted total least-squares regression line. The blue and green lines show the average TNO inventory emission ratios for the traffic and heating sector in the vicinity of Heidelberg.

Author contributions. HJ designed the study with contributions from SH, IL, and FM. FM and CR performed the flask sampling. SH and AJ provided the flask measurements. DP provided the NO_x measurements. FM conducted the modelling. HJ evaluated the data. HJ and SH wrote the manuscript with contributions from all co-authors.

Competing interests. The authors declare that they have no conflict of interest.

Disclaimer.

Acknowledgements. We thank the staff of the ICOS Central Radiocarbon Laboratory (CRL) for conducting the continuous measurements in Heidelberg and preparing the $^{14}CO_2$ analyses. Moreover, we would like to thank Ronny Friedrich from the Curt-Engelhorn Center for

Archaeometry (CECA), who performed the AMS measurements. We thank the staff at the ICOS Flask and Calibration Laboratory (FCL) for measuring all flask concentrations. Furthermore, We thank Hugo Denier van der Gon, Ingrid Super, and the staff of the Department of Climate, Air and Sustainability at TNO in Utrecht for providing the emission inventory as well as Julia Marshall, who computed and processed the high-resolution WRF meteorology in the Rhine Valley. We further would like to thank Ida Storm and the members of the ICOS Carbon Portal for their cooperation in developing tools for estimating nuclear $^{14}CO_2$ contamination at European ICOS stations. We thank Ann-Kristin Kunz for her valuable comments on the manuscript.

This research has been supported by the German Weather Service (DWD) and the ICOS Research Infrastructure. The ICOS Central Radiocarbon Laboratory is funded by the German Federal Ministry for Transport.

References

Beirle, S.: Estimating source strengths and lifetime of Nitrogen Oxides from satellite data, PhD, University of Heidelberg, Heidelberg, https://doi.org/10.11588/heidok.00005225, 2004.

Beirle, S., Platt, U., Wenig, M., and Wagner, T.: Weekly cycle of NO_2 by GOME measurements: a signature of anthropogenic sources, Atmospheric Chemistry and Physics, 3, 2225–2232, https://doi.org/10.5194/acp-3-2225-2003, 2003.

Ciais, P., Crisp, D., Denier Van Der Gon, H., Engelen, R., Heimann, M., Janssens-Maenhout, G., Rayner, P., and Scholze, M.: Towards a European Operational Observing System to Monitor Fossil CO2 Emissions. Final Report from the Expert Group, European Commission: Joint Research Centre, ISBN 978-92-79- 53482-9, https://doi.org/10.2788/350433, 2015.

Dellaert, S., Super, I., Visschedijk, A., and Denier van der Gon, H.: High resolution scenarios of CO2 and CO emissions, Tech. rep., CHE deliverable D4.2, https://www.che-project.eu/sites/default/files/2019-05/CHE-D4-2-V1-0.pdf, 2019.

Denier van der Gon, H., Kuenen, J., Boleti, E., Muntean, M., Maenhout, G., Marshall, J., and Haussaire, J.-M.: Emissions and natural fluxes Dataset, Tech. rep., CHE deliverable D2.3, https://www.che-project.eu/sites/default/files/2019-01/CHE-D2-3-V1-0.pdf, 2019.

Feng, S., Jiang, F., Wang, H., Liu, Y., He, W., Wang, H., Shen, Y., Zhang, L., Jia, M., Ju, W., and Chen, J. M.: China's Fossil Fuel CO2 Emissions Estimated Using Surface Observations of Coemitted NO2, Environmental Science & Technology, https://doi.org/10.1021/acs.est.3c07756, 2024.

Gamnitzer, U., Karstens, U., Kromer, B., Neubert, R. E. M., Meijer, H. A. J., Schroeder, H., and Levin, I.: Carbon monoxide: A quantitative tracer for fossil fuel CO2?, Journal of Geophysical Research: Atmospheres, 111, https://doi.org/10.1029/2005JD006966, 2006.

Goldberg, D. L., Lu, Z., Oda, T., Lamsal, L. N., Liu, F., Griffin, D., McLinden, C. A., Krotkov, N. A., Duncan, B. N., and Streets, D. G.: Exploiting OMI NO2 satellite observations to infer fossil-fuel CO2 emissions from U.S. megacities, Science of The Total Environment, 695, 133 805, https://doi.org/10.1016/j.scitotenv.2019.133805, 2019.

Hazan, L., Tarniewicz, J., Ramonet, M., Laurent, O., and Abbaris, A.: Automatic processing of atmospheric CO_2 and CH_4 mole fractions at the ICOS Atmosphere Thematic Centre, Atmospheric Measurement Techniques, 9, 4719–4736, https://doi.org/10.5194/amt-9-4719-2016, publisher: Copernicus GmbH, 2016.

Hersbach, H., Bell, B., Berrisford, P., Hirahara, S., Horányi, A., Muñoz-Sabater, J., Nicolas, J., Peubey, C., Radu, R., Schepers, D., Simmons, A., Soci, C., Abdalla, S., Abellan, X., Balsamo, G., Bechtold, P., Biavati, G., Bidlot, J., Bonavita, M., De Chiara, G., Dahlgren, P., Dee, D., Diamantakis, M., Dragani, R., Flemming, J., Forbes, R., Fuentes, M., Geer, A., Haimberger, L., Healy, S., Hogan, R. J., Hólm, E., Janisková, M., Keeley, S., Laloyaux, P., Lopez, P., Lupu, C., Radnoti, G., De Rosnay, P., Rozum, I., Vamborg, F., Villaume, S., and Thépaut, J.: The ERA5 global reanalysis, Quarterly Journal of the Royal Meteorological Society, 146, 1999–2049, https://doi.org/10.1002/qj.3803, 2020.

Horbanski, M., Pöhler, D., Lampel, J., and Platt, U.: The ICAD (iterative cavity-enhanced DOAS) method, Atmospheric Measurement Techniques, 12, 3365–3381, https://doi.org/10.5194/amt-12-3365-2019, 2019.

ICOS RI: ICOS Atmosphere Station Specifications V2.0 (editor: O. Laurent), ICOS ERIC, https://doi.org/10.18160/GK28-2188, 2020.

Jaschke, C.: Potentials and Limitations of Proxy to Fossil Fuel CO2 Ratios – a Case Study at the ICOS Station near Karlsruhe, Master's thesis, University of Heidelberg, Heidelberg, 2021.

Jordan, A. and Damak, F.: ICOS CAL - Quality Control Report 2024, ICOS CAL, https://doi.org/10.18160/V2NS-9WXH, 2025.

Kenagy, H. S., Sparks, T. L., Ebben, C. J., Wooldrige, P. J., Lopez-Hilfiker, F. D., Lee, B. H., Thornton, J. A., McDuffie, E. E., Fibiger, D. L., Brown, S. S., Montzka, D. D., Weinheimer, A. J., Schroder, J. C., Campuzano-Jost, P., Day, D. A., Jimenez, J. L., Dibb, J. E., Campos,

T., Shah, V., Jaeglé, L., and Cohen, R. C.: NOx Lifetime and NOy Partitioning During WINTER, Journal of Geophysical Research: Atmospheres, 123, 9813–9827, https://doi.org/10.1029/2018JD028736, 2018.

Konovalov, I. B., Berezin, E. V., Ciais, P., Broquet, G., Zhuravlev, R. V., and Janssens-Maenhout, G.: Estimation of fossil-fuel CO_2 emissions using satellite measurements of "proxy" species, Atmospheric Chemistry and Physics, 16, 13 509–13 540, https://doi.org/10.5194/acp-16-13509-2016, 2016.

Kromer, B. and Münnich, K. O.: Co2 Gas Proportional Counting in Radiocarbon Dating — Review and Perspective, in: Radiocarbon After Four Decades, edited by Taylor, R. E., Long, A., and Kra, R. S., pp. 184–197, Springer, New York, NY, ISBN 978-1-4757-4249-7, https://doi.org/10.1007/978-1-4757-4249-7_13, 1992.

Kromer, B., Lindauer, S., Synal, H.-A., and Wacker, L.: MAMS – A new AMS facility at the Curt-Engelhorn-Centre for Achaeometry, Mannheim, Germany, Nuclear Instruments and Methods in Physics Research Section B: Beam Interactions with Materials and Atoms, 294, 11–13, https://doi.org/10.1016/j.nimb.2012.01.015, 2013.

Levin, I. and Karstens, U.: Inferring high-resolution fossil fuel CO2 records at continental sites from combined 14CO2 and CO observations, Tellus B: Chemical and Physical Meteorology, 59, 245, https://doi.org/10.1111/j.1600-0889.2006.00244.x, 2007.

Levin, I., Münnich, K. O., and Weiss, W.: The Effect of Anthropogenic CO2 and 14C Sources on the Distribution of 14C in the Atmosphere, Radiocarbon, 22, 379–391, https://doi.org/10.1017/S003382220000967X, 1980.

Levin, I., Kromer, B., Schmidt, M., and Sartorius, H.: A novel approach for independent budgeting of fossil fuel CO2 over Europe by 14CO2 observations, Geophysical Research Letters, 30, https://doi.org/10.1029/2003GL018477, 2003.

Levin, I., Karstens, U., Eritt, M., Maier, F., Arnold, S., Rzesanke, D., Hammer, S., Ramonet, M., Vítková, G., Conil, S., Heliasz, M., Kubistin, D., and Lindauer, M.: A dedicated flask sampling strategy developed for Integrated Carbon Observation System (ICOS) stations based on CO_2 and CO measurements and Stochastic Time-Inverted Lagrangian Transport (STILT) footprint modelling, Atmospheric Chemistry and Physics, 20, 11 161–11 180, https://doi.org/10.5194/acp-20-11161-2020, 2020.

Lin, J. C., Gerbig, C., Wofsy, S. C., Andrews, A. E., Daube, B. C., Davis, K. J., and Grainger, C. A.: A near-field tool for simulating the upstream influence of atmospheric observations: The Stochastic Time-Inverted Lagrangian Transport (STILT) model, Journal of Geophysical Research: Atmospheres, 108, https://doi.org/10.1029/2002JD003161, 2003.

Ling, Q., Zhou, Y., Chen, D., Varricchio, L., Detti, A., Bartalini, S., and Guan, Z.: Laser spectroscopy applied in radiocarbon dating with the bomb peak, Optics Express, 33, 7830, https://doi.org/10.1364/OE.554129, 2025.

Liu, F., Beirle, S., Zhang, Q., Dörner, S., He, K., and Wagner, T.: NO_x lifetimes and emissions of cities and power plants in polluted background estimated by satellite observations, Atmospheric Chemistry and Physics, 16, 5283–5298, https://doi.org/10.5194/acp-16-5283-2016, 2016.

Liu, F., Duncan, B. N., Krotkov, N. A., Lamsal, L. N., Beirle, S., Griffin, D., McLinden, C. A., Goldberg, D. L., and Lu, Z.: A methodology to constrain carbon dioxide emissions from coal-fired power plants using satellite observations of co-emitted nitrogen dioxide, Atmospheric Chemistry and Physics, 20, 99–116, https://doi.org/10.5194/acp-20-99-2020, 2020.

Lopez, M., Schmidt, M., Delmotte, M., Colomb, A., Gros, V., Janssen, C., Lehman, S. J., Mondelain, D., Perrussel, O., Ramonet, M., Xueref-Remy, I., and Bousquet, P.: CO, NO_x and $^{13}CO_2$ as tracers for fossil fuel CO_2: results from a pilot study in Paris during winter 2010, Atmospheric Chemistry and Physics, 13, 7343–7358, https://doi.org/10.5194/acp-13-7343-2013, 2013.

Lux, J. T.: A new target preparation facility for high precision AMS measurements and strategies for efficient 14CO2 sampling, PhD, University of Heidelberg, Heidelberg, https://doi.org/10.11588/heidok.00024767, 2018.

Maier, F.: Estimating fossil fuel carbon dioxide (ffCO2) emissions in the Rhine Valley metropolitan region from local atmospheric observations in Heidelberg, PhD, University of Heidelberg, Heidelberg, 2023.

Maier, F., Gerbig, C., Levin, I., Super, I., Marshall, J., and Hammer, S.: Effects of point source emission heights in WRF–STILT: a step towards exploiting nocturnal observations in models, Geoscientific Model Development, 15, 5391–5406, https://doi.org/10.5194/gmd-15-5391-2022, 2022.

Maier, F., Levin, I., Gachkivskyi, M., Rödenbeck, C., and Hammer, S.: Estimating regional fossil fuel CO2 concentrations from 14CO2 observations: challenges and uncertainties, Philosophical Transactions of the Royal Society A: Mathematical, Physical and Engineering Sciences, 381, 20220 203, https://doi.org/10.1098/rsta.2022.0203, 2023.

Maier, F., Levin, I., Conil, S., Gachkivskyi, M., Denier van der Gon, H., and Hammer, S.: Uncertainty in continuous ΔCO-based $\Delta ffCO_2$ estimates derived from ^{14}C flask and bottom-up ΔCO / $\Delta ffCO_2$ ratios, Atmospheric Chemistry and Physics, 24, 8205–8223, https://doi.org/10.5194/acp-24-8205-2024, 2024a.

Maier, F., Rödenbeck, C., Levin, I., Gerbig, C., Gachkivskyi, M., and Hammer, S.: Potential of ^{14}C-based vs. ΔCO-based $\Delta ffCO_2$ observations to estimate urban fossil fuel CO_2 ($ffCO_2$) emissions, Atmospheric Chemistry and Physics, 24, 8183–8203, https://doi.org/10.5194/acp-24-8183-2024, 2024b.

Martin, R. V., Jacob, D. J., Chance, K., Kurosu, T. P., Palmer, P. I., and Evans, M. J.: Global inventory of nitrogen oxide emissions constrained by space-based observations of NO2 columns, Journal of Geophysical Research: Atmospheres, 108, https://doi.org/10.1029/2003JD003453, 2003.

Nehrkorn, T., Eluszkiewicz, J., Wofsy, S. C., Lin, J. C., Gerbig, C., Longo, M., and Freitas, S.: Coupled weather research and forecasting–stochastic time-inverted lagrangian transport (WRF–STILT) model, Meteorology and Atmospheric Physics, 107, 51–64, https://doi.org/10.1007/s00703-010-0068-x, 2010.

Romer, P. S., Duffey, K. C., Wooldridge, P. J., Allen, H. M., Ayres, B. R., Brown, S. S., Brune, W. H., Crounse, J. D., De Gouw, J., Draper, D. C., Feiner, P. A., Fry, J. L., Goldstein, A. H., Koss, A., Misztal, P. K., Nguyen, T. B., Olson, K., Teng, A. P., Wennberg, P. O., Wild, R. J., Zhang, L., and Cohen, R. C.: The lifetime of nitrogen oxides in an isoprene-dominated forest, Atmospheric Chemistry and Physics, 16, 7623–7637, https://doi.org/10.5194/acp-16-7623-2016, 2016.

Super, I., Denier van der Gon, H. A. C., van der Molen, M. K., Dellaert, S. N. C., and Peters, W.: Optimizing a dynamic fossil fuel CO_2 emission model with CTDAS (CarbonTracker Data Assimilation Shell, v1.0) for an urban area using atmospheric observations of CO_2, CO, NO_x, and SO_2, Geoscientific Model Development, 13, 2695–2721, https://doi.org/10.5194/gmd-13-2695-2020, 2020.

Super, I., Scarpelli, T., Droste, A., and Palmer, P. I.: Improved definition of prior uncertainties in CO_2 and CO fossil fuel fluxes and its impact on multi-species inversion with GEOS-Chem (v12.5), Geoscientific Model Development, 17, 7263–7284, https://doi.org/10.5194/gmd-17-7263-2024, 2024.

Turnbull, J. C., Miller, J. B., Lehman, S. J., Tans, P. P., Sparks, R. J., and Southon, J.: Comparison of 14CO2, CO, and SF6 as tracers for recently added fossil fuel CO2 in the atmosphere and implications for biological CO2 exchange, Geophysical Research Letters, 33, https://doi.org/10.1029/2005GL024213, 2006.

Turnbull, J. C., Sweeney, C., Karion, A., Newberger, T., Lehman, S. J., Tans, P. P., Davis, K. J., Lauvaux, T., Miles, N. L., Richardson, S. J., Cambaliza, M. O., Shepson, P. B., Gurney, K., Patarasuk, R., and Razlivanov, I.: Toward quantification and source sector identification of fossil fuel CO2 emissions from an urban area: Results from the INFLUX experiment, Journal of Geophysical Research: Atmospheres, 120, 292–312, https://doi.org/10.1002/2014JD022555, 2015.

Van Der Laan, S., Karstens, U., Neubert, R., Van Der Laan-Luijkx, I., and Meijer, H.: Observation-based estimates of fossil fuel-derived CO_2 emissions in the Netherlands using Δ14C, CO and ^{222}Radon, Tellus B: Chemical and Physical Meteorology, 62, 389, https://doi.org/10.1111/j.1600-0889.2010.00493.x, 2010.